Nature of weak generalized synchronization in chaotically driven maps

Gerhard Keller,[1] Haider H. Jafri,[2] and Ram Ramaswamy[2,3]
[1]*Department of Mathematics, Universität Erlangen-Nürnberg, Cauerstrasse 11, 91058 Erlangen, Germany*
[2]*School of Physical Sciences, Jawaharlal Nehru University, New Delhi 110067, India*
[3]*University of Hyderabad, Hyderabad 500 046, India*
(Received 21 December 2012; published 12 April 2013)

Weak generalized synchrony in a drive-response system occurs when the response dynamics is a unique but nondifferentiable function of the drive, in a manner that is similar to the formation of strange nonchaotic attractors in quasiperiodically driven dynamical systems. We consider a chaotically driven monotone map and examine the geometry of the limit set formed in the regime of weak generalized synchronization. The fractal dimension of the set of zeros is studied both analytically and numerically. We further examine the stable and unstable sets formed and measure the regularity of the coupling function. The stability index as well as the dimension spectrum of the equilibrium measure can be computed analytically.

DOI: 10.1103/PhysRevE.87.042913 PACS number(s): 05.45.Ac, 05.45.Pq, 05.45.Xt

I. INTRODUCTION

Although the subject of synchronization traces its origins to the observations of Huygens [1] on coupled nonlinear oscillators—namely pendulums suspended on a beam—the recent surge of interest in the subject largely owes itself to a number of developments in nonlinear science. Discoveries of chaotic synchronization [2–4] and of collective behavior [5], for instance, have enlarged the setting in which synchrony is discussed, bringing highly nonlinear, aperiodic, and strongly coupled systems into the ambit. This has helped to identify synchrony as an instance of an emergent phenomenon with parallels to bifurcations and phase transitions.

There are, typically, three very general scenarios within which synchrony (in its several variants) is currently discussed. Driven systems, or the so-called master-slave configurations [3] wherein both the drive and response are identical nonlinear systems can, under conditions that are well understood [6] display perfect synchrony. Systems that are mutually coupled [7] can also display perfect synchrony, depending on the coupling strength as well as on the form of the coupling. Another common scenario when two systems can show synchrony is when they are both coupled to a third.

Within these different paradigms a number of types of synchrony have also been discussed. When all the variables of the two systems coincide, they are said to be in complete or exact synchrony. If they coincide at different times, they are in lag synchrony, and if the phase difference of their oscillations remains bounded (regardless of the amplitude variations) then the systems are said to be in phase synchrony. In all these cases, the synchronizing systems are considered to be similar to one another, namely identical or nearly identical.

The notion of a *generalized* synchrony was first introduced [8] to consider the dynamics when one system is driven by another dissimilar one, and to address the question of whether there was some sense in which the two systems could be said to be synchronized or correlated. In the simplest case, given a drive with dynamics

$$\dot{\mathbf{u}} = \mathcal{F}(\mathbf{u}) \tag{1}$$

and a response system

$$\dot{\mathbf{x}} = \mathcal{G}(\mathbf{x},\mathbf{u}), \tag{2}$$

the state of generalized synchrony is the condition that the response is uniquely a function of the drive, namely

$$\mathbf{x} = \mathbf{\Phi}[\mathbf{u}] \tag{3}$$

where $\mathcal{F}$ and $\mathcal{G}$ are taken to be smooth and differentiable. The notion of generalized synchronization does of course extend beyond the master-slave scenario described above; with bidirectional coupling between the $\mathbf{u}$ and $\mathbf{x}$ subsystems, the condition (3) needs to be expanded appropriately [9]. Further, depending on whether the functional $\mathbf{\Phi}$ is differentiable or not, the generalized synchronization is further classified as strong or weak [10,11].

An example of generalized synchrony is provided in quasiperiodically driven nonlinear dynamical systems [12,13]. In this situation, the drive dynamics Eq. (1) is such that the motion is quasiperiodic; for suitable coupling, it is known that this can drive the response dynamics to an attractor on which all Lyapunov exponents are nonpositive. The unique functional dependence of the response variables on the drive, namely (3) and the associated issues of the invertibility as well as that of the differentiability of the function $\mathbf{\Phi}$ have been studied in detail. When the equations of motion of the response are appropriately nonlinear, the nonpositive Lyapunov exponents can nevertheless give rise to nontrivial quasiperiodic response dynamics if the (implicit) function $\mathbf{\Phi}$ is nondifferentiable, namely when there are strange nonchaotic attractors (SNAs). Furthermore, SNAs are known to be created via a number of distinct bifurcation routes, many of which have parallels to bifurcation phenomena in autonomous nonlinear dynamical systems.

When the drive dynamics is chaotic, there are analogies with the case of a quasiperiodic drive [14]. The nondifferentiability of the function $\mathbf{\Phi}$ can also be observed to occur through bifurcations that appear to be very similar to those in the case of SNAs, and this leads to the interesting and open question of the nature of generalized synchrony in chaotically driven nonlinear systems. Specifically, the properties of $\mathbf{\Phi}$ are of interest in the case when all the conditional Lyapunov exponents of the response system are nonpositive.

In the present work we focus on a specific (but representative) example, similar to what has been studied in detail in the context of SNAs. For instance the dynamical system

$$x_{n+1} = f(x_n,u_n) = 2r \tanh x_n \cos 2\pi u_n, \tag{4}$$

where u has the dynamics

$$u_{n+1} = u_n + 2\pi\omega \pmod{2\pi} \tag{5}$$

with ω irrational [typically taken in numerical studies to be the inverse golden mean ratio, $(\sqrt{5}-1)/2$)] has been studied extensively. In this system, there is a transition to SNA: for $r \leqslant 1$ the attractor is the line $x = 0$ and there is a blowout bifurcation at $r = 1$, above which the attractor is strange, with points on the line, as well as off the line. Here the existence of an attractor that is both nonchaotic and strange can be rigorously established [12,15,16]. As was subsequently shown by Sturman and Stark [17], any strange compact invariant set for a quasiperiodically forced system supports an invariant measure with a non-negative maximal Lyapunov exponent in the fiber (namely transverse) direction, i.e., it must contain some nonattracting orbit. SNAs have been numerically studied in a number of other systems, and are known to also be created through other, different, bifurcations [18–21].

While the aperiodicity of the drive u is essential for the strangeness, the nonchaoticity, namely the nonpositive transverse Lyapunov exponent does not require a quasiperiodic drive. In particular, a chaotic drive can also lead to a negative transverse Lyapunov exponent in essentially the same manner as in quasiperiodically driven systems [14]. If one takes u to be the output of a Baker's map, namely

$$\begin{aligned} u_{n+1} &= \begin{cases} au_n & \text{if } v_n < a \\ a + (1-a)u_n & \text{if } v_n \geqslant a \end{cases} \\ v_{n+1} &= \begin{cases} v_n/a & \text{if } v_n \leqslant a \\ (v_n - a)/(1-a) & \text{if } v_n > a, \end{cases} \end{aligned} \tag{6}$$

with a between 0 and 1, typical orbits are chaotic and uniformly distributed on the interval. Numerical computations [14] verify that the resulting *subsystem* Lyapunov exponent is negative, and the functional dependence of x on u is nonsmooth, namely it is nondifferentiable above $r = 1$; a typical orbit is shown in Fig. 1 in the regime of this "weak" GS. The similarity of the two scenarios suggests that there could be a deeper connection between the systems.

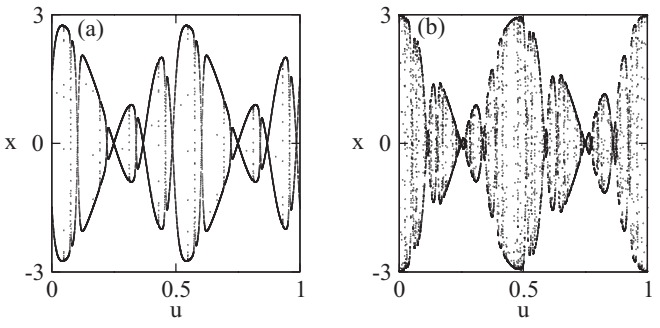

FIG. 1. (a) Limit set for the system defined by Eq. (4) at $r = 1.5$ when u_n is (a) a quasiperiodic drive [Eq. (5)] and (b) a chaotic drive taken from the Baker's map [Eq. (6)]. These calculations have been done at 500-digit precision.

Thus the main motivation of the present work is the question: to what extent can the results obtained in the case of a quasiperiodic drive be generalized to the class of chaotically driven systems? In the following section we therefore introduce a class of chaotically driven maps and study the properties of its zeros. The fractal dimension of the set of zeros is estimated analytically and is shown to be in good agreement with numerically computed values. In Sec. IV, we study a measure of the regularity of the attractor, further examining its stable and unstable sets. Finally in Sec. V, we summarize the main results of this work.

II. CHAOTICALLY DRIVEN MONOTONE MAPS

We study the transition to generalized synchronization in a drive-response system with the generalized Baker's map $F(u,v)$ above as drive and a response

$$G_r(u,x) = rg(u)h(x), \tag{7}$$

where u is the stable coordinate of the Baker's map. The multiplier $g(u)$ is a strictly positive, smooth function of the drive, and $h : [0,\infty) \to [0,\infty)$ is a bounded, increasing, strictly concave function with $h(0) = 0$ and $h'(0) = 1$. We take $h(x) = \tanh(x)$, and

$$g(u) = 1 + \epsilon + \cos(2\pi u). \tag{8}$$

Knowing only u_0 one can recover the full past of the u process applying the map $\tau : [0,1] \to [0,1]$,

$$\tau(u) = \begin{cases} u/a & \text{if } u < a \\ (u-a)/(1-a) & \text{if } u \geqslant a \end{cases} \tag{9}$$

repeatedly. Indeed, $u_{-n} = \tau^n(u_0)$ for all n $\geqslant 0$.

We find the following scenario when the parameter r is increased from 0 to high positive values: For each value of the parameter there is a coupling function $\Phi_r(u)$ that synchronizes x with the drive so that $x = \Phi_r(u)$ in the stationary regime.

When r is smaller than a first critical parameter r_0, then $\Phi_r(u) = 0$ for every u, so there is no nontrivial synchronization at all. Above this value, when r is between r_0 and a second critical parameter r_w, the identity $\Phi_r(u) = 0$ is violated on a set of u of positive Hausdorff dimension but of Lebesgue measure zero, which means that nontrivial synchronization may occur but is hardly visible in simulations. Further increasing r above r_w results in a highly irregular coupling function $\Phi_r(u)$ that has a dense set of zeros but is positive for almost all u, so one observes weak generalized synchronization [10]. This second critical transition is illustrated in Figs. 2(b)–2(d). Finally, increasing r above a third critical parameter r_s results in strong generalized synchronization in the sense that $\Phi_r(u)$ is now a strictly positive, smooth and nonconstant function of u. In mathematical terms the function $\Phi_r(u)$ is defined below in Eq. (10).

We focus on the fine structure of the coupling function $\Phi_r(u)$ in the weak synchronization regime. This function has two particularly noteworthy properties, firstly that the set N_r of its zeros is dense in the interval $[0,1]$. Even more, it is a dense G_δ set, namely it is the intersection of a countable decreasing

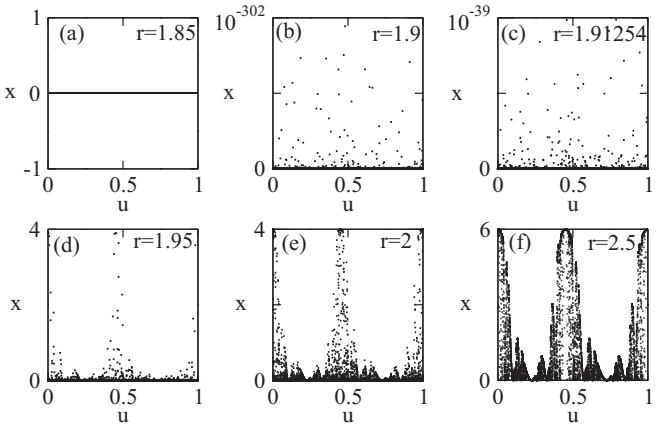

FIG. 2. Limit set for the system $x_{n+1} = f_{r,u_n}(x_n) = rg(u_n)\tanh(x_n)$ with $g(u) = 1 + \epsilon + \cos(2\pi u)(\epsilon = 0.001)$ at different parameter values r, u is the chaotic drive taken from the Baker's map [Eq. (6)]. The value of the critical parameter is $r_w = 1.91254$. All calculations have been carried out at 500-digit precision.

sequence of open dense sets. It should be noted that none of these zeros is created by a zero value of the multiplier function $g(u)$. On the other hand, the set N_r has zero Lebesgue measure so that the coupling function $\Phi_r(u)$ is positive for Lebesgue almost all u.

Therefore the fractal and self-similar structure of the graph of $\Phi_r(u)$ in a small neighborhood of the baseline $x = 0$ in the full phase space is of particular interest. In this note we propose to study the r dependence of this structure in two related ways. We first evaluate the dimension of the set N_r of zeros numerically using a formula derived in Ref. [22] from thermodynamic formalism [23,24]. Based on the statistics of long orbits we estimate the stability index of $\Phi_r(u)$ along the baseline $x = 0$ and in particular the values of the index that prevail on N_r. This index was introduced in Ref. [25] to measure the stability of an individual point on an irregular boundary of a basin of attraction by evaluating the fraction that the basin occupies in small neighborhoods of the given point. Here we evaluate instead the fraction that the system's global attractor, which is just the area below the graph of $\Phi_r(u)$, occupies in small neighborhoods of points of the baseline. Although the index measures rather the regularity of $\Phi_r(u)$ than its stability, we adhere to the name given in Ref. [25]. Our numerical findings match the predictions made in Ref. [26] quite well.

III. DIMENSION OF SET OF ZEROES

A. Background on the thermodynamic formalism

The set $N_r = \{u : \Phi_r(u) = 0\}$ of zeros of Φ_r is easily seen to be invariant under the driving dynamics and hence also under the map τ. Therefore it has measure 0 or 1 for each ergodic invariant measure of τ. In particular, as the Lebesgue measure is ergodic and invariant under τ, it is a Lebesgue null set whenever r is between r_w and r_s.

The values $\Phi_r(u)$ can be defined by a pullback construction: For each sufficiently large starting value $z > 0$, one has

$$\Phi_r(u) = \lim_{n\to\infty} f^n_{r,u}(z), \text{ where}$$
$$f^n_{(r,u)}(z) := f_{r,u_{-1}}\{f_{r,u_{-2}}[\ldots f_{r,u_{-n}}(z)\ldots]\} \tag{10}$$

and $u_{-i} = \tau^i(u)$. Explicitly, $f^2_{r,u}(z) = f_{r,u_{-1}}[f_{r,u_{-2}}(z)]$, $f^3_{r,u}(z) = f_{r,u_{-1}}\{f_{r,u_{-2}}[f_{r.u_{-3}}(z)]\}$ and so on. This is a variant of the usual pullback construction, see, e.g., Ref. [15]. As these pullback orbits spend most of the time close to zero when their limit $\Phi_r(u)$ is equal to 0, it is plausible that N_r coincides essentially with the set of all u for which the pullback Lyapunov exponent in fiber direction at $(u,0)$ defined by

$$\Gamma(r,u) = \lim_{n\to\infty}\frac{1}{n}\ln\left(f^n_{r,u}\right)'(0) = \ln r + \lim_{n\to\infty}\frac{1}{n}\sum_{i=1}^{n}\ln g(u_{-i}) \tag{11}$$

is not positive. Indeed, one can show [22] that there is a unique invariant probability measure μ_r supported on N_r for which $\int \Gamma(r,u)d\mu_r(u) = 0$ and which is the unique measure of maximal Hausdorff dimension among all invariant probabilities supported on N_r. The Hausdorff dimension $d_H(\mu_r)$ of this measure coincides with that of the set N_r, and in the rest of this section we will concentrate on the numerical determination of $d_H(\mu_r)$.

The measure μ_r can be explicitly constructed as the unique equilibrium measure $\mu_{\eta,\beta}$ for the potential $-\eta\ln\tau' + \beta\ln(rg)$ where $\eta = \eta(r)$ and $\beta = \beta(r)$ are determined such that its average Lyapunov exponent in fiber direction

$$\Gamma(r,\mu_{\eta,\beta}) := \int \Gamma(r,u)d\mu_{\eta,\beta}(u) = \ln r + \int \ln g(u)\,d\mu_{\eta,\beta}(u) \tag{12}$$

is zero and its free energy is zero as well. Hence the two parameters η and β are the solution to two equations

$$\int \ln g(u)\,d\mu_{\eta,\beta}(u) = -\ln r \tag{13}$$

and

$$\mathrm{P}_{\mathrm{top}}[-\eta\ln\tau' + \beta\ln(rg)] = 0, \tag{14}$$

where $\mathrm{P}_{\mathrm{top}}(\psi)$ denotes the topological pressure (also called free energy) of a potential ψ. By the variational principle,

$$\mathrm{P}_{\mathrm{top}}[-\eta\ln\tau' + \beta\ln(rg)] = \max_{\mu}\{h_{KS}(\mu) - \eta\Lambda(\mu) + \beta\Gamma(r,\mu)\} \tag{15}$$

where the maximum extends over all τ-invariant probabilities μ,

$$\Lambda(\mu) = \int \ln\tau'(u)\,d\mu(u) \tag{16}$$

is the Lyapunov exponent of τ under μ, and $h_{KS}(\mu)$ denotes the Kolmogorov-Sinai entropy of (τ,μ) [27]. The equilibrium measure $\mu_{\eta,\beta}$ is the unique invariant probability measure for which the maximum in Ref. (15) is attained.

As $\Gamma(r,\mu_{\eta,\beta}) = 0$, Eqs. (14) and (15) imply that $h_{KS}(\mu_{\eta,\beta}) - \eta\Lambda(\mu_{\eta,\beta}) = 0$, so that finally the identity "entropy

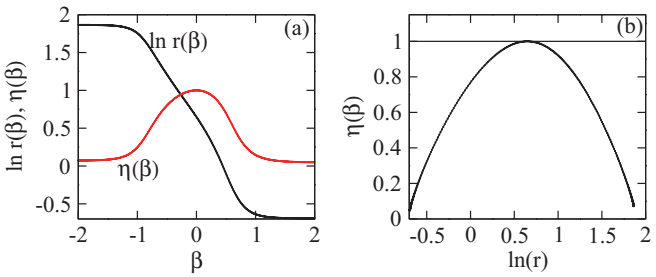

FIG. 3. (Color online) (a) $\ln r$ and η as functions of β. (b) Implicit plot of $\eta(\beta) = d_H(N_{r(\beta)})$ versus $\ln r(\beta)$. The maximum value $\eta(\beta) = 1$ is reached for $\beta = 0$ at $\ln r(\beta) = \ln r_w = 0.648428$, compare this to the theoretical value $\ln[2/(1+\epsilon+\sqrt{2\epsilon+\epsilon^2})] = 0.648430$ for $\epsilon = 0.001$.

equals dimension times Lyapunov exponent" yields

$$d_H(N_r) = d_H(\mu_r) = \frac{h_{KS}(\mu_{\eta(r),\beta(r)})}{\Lambda(\mu_{\eta(r),\beta(r)})} = \eta(r). \tag{17}$$

This identity, in its simplest form, goes back to work of Besicovich, Eggleston, and Billingsley [28], but see also Ref. [29] for a more recent account. For a particular system the function $\eta(r)$ is depicted in Fig. 3. It was mathematically investigated in Ref. [22] where it was proved that it is real analytic and unimodal on the interval (r_0, r_s) with a unique maximum at r_w. There is no mathematical proof that its limiting values $\eta(r_0)$ and $\eta(r_s)$ are always identically zero, but see Sec. III C for a discussion of the system in Fig. 3.

B. Determining $d_H(N_r)$

Denote by $u^{(1)}, u^{(2)}, \ldots, u^{(2^N)}$ the collection of the 2^N fix points of the map τ^N. These are all periodic points of τ whose minimal period divides N. Let $\phi_N(u) = \sum_{i=0}^{N-1} \ln \tau'(\tau^i u)$ and $\psi_N(u) = \sum_{i=0}^{N-1} \ln g(\tau^i u)$. With these conventions we define

$$\mu_{\eta,\beta}^N = \frac{1}{Z_N(\eta,\beta)} \sum_{j=1}^{2^N} e^{-\eta\phi_N(u^{(j)})+\beta\psi_N(u^{(j)})} \delta_{u^{(j)}}, \tag{18}$$

where $Z_N(\eta,\beta) = \sum_{j=1}^{2^N} e^{-\eta\phi_N(u^{(j)})+\beta\psi_N(u^{(j)})}$ is the partition function. As equilibrium measures $\mu_{\eta,\beta}$ are very well approximated by convex combinations of Dirac measures on periodic points [30], Eq. (13) can be replaced, for numerical purposes, by

$$\frac{1}{Z_N(\eta,\beta)} \sum_{j=1}^{2^N} e^{-\eta\phi_N(u^{(j)})+\beta\psi_N(u^{(j)})} \ln g(u^{(j)}) = -\ln r \tag{19}$$

and as $N^{-1} \ln Z_N(\eta,\beta) + \beta \ln r$ converges to the pressure from (14) in the limit $N \to \infty$, equation (14) can be replaced by

$$N^{-1} \ln Z_N(\eta,\beta) + \beta \ln r = 0. \tag{20}$$

For both equations, N has to be sufficiently large; note that the number of point masses in $\mu_{\eta,\beta}^N$ is 2^N.

Combining (19) and (20) leads to the following equation that does not involve the parameter r and can be solved numerically for η when β is given,

$$\frac{1}{Z_N(\eta,\beta)} \sum_{j=1}^{2^N} e^{-\eta\phi_N(u^{(j)})+\beta\psi_N(u^{(j)})} \ln g(u^{(j)}) = \frac{\ln Z_N(\eta,\beta)}{N\beta}. \tag{21}$$

Knowing $\eta(\beta)$, equation (20) yields at once the value of the corresponding parameter $r(\beta)$. As each point $u^{(j)}$ is represented by exactly one of the 2^N symbolic 0-1 sequences of length N, the values of the $u^{(j)}$ can be determined efficiently and to high precision by iterating backwards the inverses of the corresponding branches of τ.

For the system described in Eqs. (8) and (9) with parameters $a = 0.45$ and $\epsilon = 0.001$, the $\eta(r)$ curve is displayed in Fig. 3. Observe that the maximal dimension $d_H(N_r) = \eta(r)$ is 1 and that it is attained when $\ln r = 0.648428$. This is the parameter r_w where the graph of $\Phi_r(u)$ starts to detach from the baseline. Its numerically determined value is in excellent agreement with the precise value $\ln r_w = -\int_0^1 \ln g(u)\,du = -\int_0^1 \ln[1+\epsilon+\cos(2\pi u)]\,du = \ln[2/(1+\epsilon+\sqrt{2\epsilon+\epsilon^2})] = 0.6484295$ [31]. The increasing branch of the curve in Fig. 3 is related to the size of the set $N_r^c = \{u : \Phi(u) > 0\}$ for $r < r_w$, in which case $d_H(N_r^c) = \eta(r)$ [22].

It follows from Eqs. (13)–(15) that the limiting values of $r(\beta)$ for $\beta \to \pm\infty$ are given by $\ln r(+\infty) = -\max_\mu \int \ln g\, d\mu$ and $\ln r(-\infty) = -\min_\mu \int \ln g\, d\mu$. It is not hard to see that $r(+\infty) = r_0$ and $r(-\infty) = r_s$ for the critical parameters r_0 and r_s introduced in Sec. II. For the above numerical example one calculates along the lines of Sec. III C that $\ln r_0 = -0.6936471$ and $\ln r_s = 1.865523$.

C. Apparent discontinuities at the ends of the $\eta(r)$ curve

The lower left points of the graph of $d_H(N_r)$ in Fig. 3(b) have coordinates $[r(\beta), \eta(\beta)]$ for large $\beta > 0$, and also a further increase of β leads to a saturation at $r(\beta) = r_s$ and $\eta(\beta) = N^{-1}$. At first sight one might think that the curve drops down to zero at this point. However these apparent discontinuities are due to the approximation of Eqs. (13) and (14) by (19) and (20): The function $\psi(u) = \ln[1+\epsilon+\cos(2\pi u)]$ attains its unique maximum $\ln(2+\epsilon)$ at the fixed points $u = 0$ and $u = 1$ of τ. Therefore, for each N the maximum of all values $\psi_N(u^{(j)})/N$ is attained at the fixed points $u^{(1)} = 0$ and $u^{(2^N)} = 1$. Indeed, for large $\beta > 0$ the two terms $\psi_N(u^{(1)})$ and $\psi_N(u^{(2^N)})$ dominate the sum defining $Z_N(\eta,\beta)$ completely, so that Eq. (21) reduces to

$$\ln(2+\epsilon) \approx -\frac{1}{N\beta} \ln[a^{-N\eta}(2+\epsilon)^{N\beta} + (1-a)^{-N\eta}(2+\epsilon)^{N\beta}]$$
$$= \ln(2+\epsilon) - \frac{1}{N\beta} \ln[a^{-N\eta} + (1-a)^{-N\eta}],$$

and this has the only solution $\eta = N^{-1}$.

The error in this approximation is of order $o(N)$ as has been verified numerically for different values of N from $N = 15$–24, as described in Table I. A similar analysis can be carried out for the lower right points of the graph of $d_H(N_r)$ in Fig. 3(b). For large negative β the sum is now dominated by the contributions from the three-periodic orbit

TABLE I. The η values at the left and right end of the graph in Fig. 3(b).

	Left end of curve		Right end of curve	
N	Theoretical value of $\eta = N^{-1}$ for $\beta \to \infty$	Numerical value of $\eta(\beta)$ for $\beta = 2$	Theoretical value of $\eta = N^{-1}\frac{3\ln 3}{-\ln(a^2(1-a))}$ for $\beta \to -\infty$	Numerical value of $\eta(\beta)$ for $\beta = -2$
15	0.0666	0.0666	0.1001	0.1002
18	0.0555	0.0555	0.0835	0.0835
21	0.0476	0.0476	0.0715	0.0717
24	0.0416	0.0416	0.0626	0.0628

with symbolic sequence $(001)^\infty$. When N is a multiple of 3, a similar calculation as before leads to

$$\eta = N^{-1}\,\frac{3\ln 3}{-\ln[a^2(1-a)]} \tag{22}$$

Comparison of the theoretical values and the values obtained numerically are given in Table I confirming excellent agreement.

IV. MULTIFRACTAL PROPERTIES OF THE STABILITY INDEX

A. The stability index

Podvigina and Ashwin [25] introduced a stability index to quantify the local geometry of basins of attraction close to points on the basin boundary. Here we use the same index to measure the local regularity of the coupling function $x = \Phi_r(u)$ close to the baseline $x = 0$. As the region between the baseline and the graph of $\Phi_r(u)$ is the global attractor of the system, our situation is not too different from the one in Ref. [25].

For each u let

$$\sigma(u) := \sigma_+(u) - \sigma_-(u) \tag{23}$$

where

$$\sigma_-(u) := \lim_{\epsilon\to 0}\frac{\ln \Sigma_\epsilon(u)}{\ln\epsilon} \text{ and } \sigma_+(u) := \lim_{\epsilon\to 0}\frac{\ln[1-\Sigma_\epsilon(u)]}{\ln\epsilon} \tag{24}$$

and

$$\Sigma_\epsilon(u) := \frac{1}{2\epsilon^2}\int_{u-\epsilon}^{u+\epsilon}\min\{\Phi_r(t),\epsilon\}\,dt, \tag{25}$$

When the r dependence of $\sigma(u)$ is to be emphasized, it is denoted $\sigma(r,u)$.

To motivate this index consider the simplest model situation where $\Phi_r(u) = |u|^p$, $p > 0$, for $-\epsilon \leqslant u \leqslant \epsilon$. Then

$$\Sigma_\epsilon(0) = \begin{cases} \frac{1}{2\epsilon^2}\left(2\epsilon\left(\epsilon - \epsilon^{\frac{1}{p}}\right) + \int_{-\epsilon^{1/p}}^{\epsilon^{1/p}} |u|^p\,du\right) = 1 - \frac{p}{p+1}\epsilon^{(1-p)/p} & \text{if } p \leqslant 1 \\ \frac{1}{2\epsilon^2}\int_{-\epsilon}^{\epsilon} u^p\,du = \frac{1}{p+1}\epsilon^{p-1} & \text{if } p \geqslant 1, \end{cases} \tag{26}$$

so that $\sigma(0) = (1-p)/p$ if $p \leqslant 1$ and $\sigma(0) = 1 - p$ if $p \geqslant 1$. Hence strongly negative values of the index correspond to large p for which the region between the baseline and the graph of Φ is very thin in small neighbourhoods of 0, while strongly positive values of the index correspond to p very close to zero for which this region nearly fills small neighborhoods of 0.

The index $\sigma(r,u)$ is invariant under the dynamics, i.e., $\sigma(r,\tau(u)) = \sigma(r,u)$ [25], so it is almost surely constant for each of the equilibrium measures $\mu_{\eta,\beta}$ introduced in Sec. III A. Consider now a second parameter $r' = re^{-\gamma}$. The set of points u for which $\Gamma(r,u) = \gamma = -\ln\frac{r'}{r}$ coincides with the set of points for which $\Gamma(r',u) = 0$, which in turn is well represented by the equilibrium measure $\mu_{r'} = \mu_{\eta(r'),\beta(r')}$ as argued in Sec. III A. As in Sec. III B we use β as the independent parameter and study $\mu_{r'(\beta)} = \mu_{\eta(\beta),\beta}$ and

$$\sigma_{(\pm)}(r,\beta) := \int \sigma_{(\pm)}(r,u)\,d\mu_{r'(\beta)}(u) \tag{27}$$

as a function of β. So $\sigma(r,\beta)$ is the stability index of $\Phi_r(u)$ at typical points u for which the Lyapunov exponent in fiber direction is $\Gamma(r,u) = -\ln\frac{r'(\beta)}{r}$.

B. Theoretical prediction for the stability index

Let

$$\Lambda(\beta) := \int \ln\tau'\,d\mu_{r'(\beta)} \;=\; \Lambda(\mu_{r'(\beta)}) \quad \text{and} \tag{28}$$

$$\Gamma(\beta) := \int \ln g\,d\mu_{r'(\beta)} \;=\; \Gamma(r,\mu_{r'(\beta)}) - \ln(r)\,. \tag{29}$$

It was proved in Ref. [26] that

$$\sigma(r,\beta) = \begin{cases} \sigma_+(r,\beta) = \frac{\ln r+\Gamma(\beta)+\Lambda(\beta)}{\Lambda(\beta)} s^*(r) & \text{if } \ln r + \Gamma(\beta) + \Lambda(\beta) \geqslant 0 \\ -\sigma_-(r,\beta) = \frac{\ln r+\Gamma(\beta)+\Lambda(\beta)}{\Lambda(\beta)} & \text{if } \ln r + \Gamma(\beta) + \Lambda(\beta) \leqslant 0\,. \end{cases} \tag{30}$$

(Note that in Ref. [26] the multiplicative parameter r is included in the function g.) Here $s^*(r)$ is a thermodynamic quantity, namely the unique positive zero of the function $F_r(s) = \mathrm{P}_{\mathrm{top}}[-\ln\tau' - s\ln(rg)]$. [Observe that F_r is convex, that $F_r(0) = 0$ and $F_r'(0) = -\int \ln[rg(u)]\,du < 0$ as $r > r_w$, and that $\lim_{s\to\infty} F_r(s) = \infty$ as $r < r_s$.]

Replacing $F_r(s)$ and the equilibrium measure $\mu_{r'(\beta)}$ by their periodic orbit approximations $N^{-1}\ln Z_N(-1,-s)$ and $\mu^N_{\eta(\beta),\beta}$ from (18) and (20), respectively, one can compute $\Lambda(\beta)$ and $\Gamma(\beta)$ to high precision and determine $\sigma(r,\beta)$ as a function of β. For the particular system defined in (8) and (9) and with parameters $a = 0.45$, $\epsilon = 0.001$, and $r = 2$, this curve is displayed in Fig. 4. The approximation is based on all 2^{21} fixed points of the map τ^N, $N = 21$, The critical value for β where $\ln r + \Gamma(\beta) + \Lambda(\beta) = 0$ is denoted by β_r; to approximate it numerically is straightforward.

C. Computation of the stability index $\sigma(r,\beta)$

In this section we describe a numerical procedure to estimate $\sigma(r,\beta)$ from its definition, and we compare the results to the theoretical predictions reported in Sec. IV B.

As the numerical computation of $\sigma_-(r,u) = \lim_{\epsilon\to 0}\frac{\ln\Sigma_\epsilon(u)}{\ln\epsilon}$ from (24) for individual points u is rather unfeasible, we replace a direct estimate of $\sigma_-(r,\beta) = \int \sigma_-(r,u)\,d\mu_{r'(\beta)}(u)$ by an estimate of $\lim_{\epsilon\to 0}\frac{1}{\ln\epsilon}\ln\int\Sigma_\epsilon(u)\,d\mu_{r'(\beta)}(u)$. This involves, on the one hand, an interchange of the limit and the integral, which we take for granted, because numerical computations are based on finite positive ϵ anyway. On the other hand, it involves an interchange of the integral and the logarithm, which has the potential to distort our estimates. This difficulty is resolved by truncating the $\Sigma_\epsilon(u)$ values at the 80% level, a procedure that was justified and shown to work properly in the related situation of estimating the information dimension of a distribution [32]. For computational purposes we also replace the $\Sigma_\epsilon(u)$ by values $\Sigma'_\epsilon(u)$, which are defined just like the $\Sigma_\epsilon(u)$ in (25) but replacing the integration interval $(u-\epsilon, u+\epsilon)$ centered at u by that interval of a 2ϵ grid, which contains the point u.

In this way we approximate the integrals $\int\Sigma'_\epsilon(u)\,d\mu_{r'(\beta)}(u)$ for a scale of ϵ values and determine the slope $s_-(r,\beta)$ of the graph of $\ln\int\Sigma'_\epsilon(u)\,d\mu_{r'(\beta)}(u)$ as a function of $\ln\epsilon$ by the method of least squares. This is our numerical approximation to $\sigma_-(r,\beta)$. In an analogous way a numerical approximation $s_+(r,\beta)$ of $\sigma_+(r,\beta)$ is determined.

In order to calculate $\int\Sigma'_\epsilon(u)\,d\mu_{r'(\beta)}(u)$ numerically, we replace again the measure $\mu_{r'(\beta)} = \mu_{\eta(\beta),\beta}$ by its periodic point approximation $\mu^N_{\eta(\beta),\beta}$ from (20). The quantities $\Sigma'_\epsilon(u) = \frac{1}{2\epsilon^2}\int_{I_k}\min\{\Phi_r(t),\epsilon\}\,dt$ are approximated by numbers $S_\epsilon(u)$ as follows. Denote by $I_1,\ldots,I_M$ the intervals of a 2ϵ grid of $[0,1]$. Suppose $u\in I_k$. To calculate the $S_\epsilon(u)$, we choose a random point $v\in[0,1]$ and a large integer L and sum up all values $\Phi_r(\tau^j v)$ $(j = 1,\ldots,L)$ for which $\tau^j v\in I_k$ and $\Phi_r(\tau^j v)\leqslant\epsilon$, and add ϵ for each $\tau^j v\in I_k$ for which $\Phi_r(\tau^j v) > \epsilon$. Once this sum is calculated, it is normalized. (Observe that the orbit $(\tau^j v)_{j\in\mathbb{N}}$ of a typical point $v\in[0,1]$ is equidistributed in $[0,1]$.)

Putting everything together we obtain the following approximation to $\sigma(r,\beta)$:

$$\tilde{s}(r,\beta) := \begin{cases} -s_-(r,\beta) & \text{if } \beta < \beta_r \\ s_+(r,\beta) & \text{if } \beta > \beta_r. \end{cases} \tag{31}$$

It is plotted in Fig. 4(a) together with the predicted values from Sec. IV B, and as can be seen, the agreement is quite satisfactory.

Although we do not undertake a full multifractal analysis of the stability index in this paper, we present in Fig. 4(b) a plot of the dimension $\eta(\sigma)$ of that equilibrium measure $\mu_{r'(\beta)}$ that realizes the stability index $\sigma = \sigma(r,\beta)$ with $r = 2$, see (27). If the slope of τ were equal to $a^{-1} = 2$, this would precisely be the dimension of all points with index σ; here this dimension will deviate slightly from the one in Fig. 4(b).

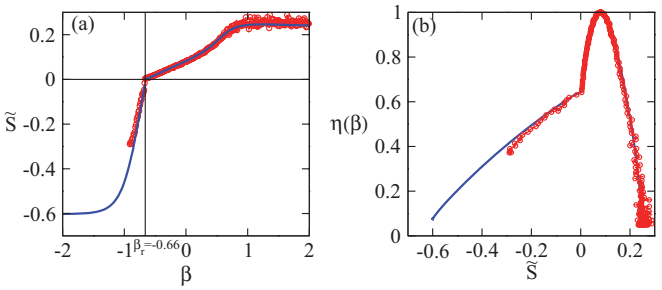

FIG. 4. (Color online) (a) The stability index $\sigma(r,\beta)$ as a function of β (blue line) and its direct numerical approximation $\tilde{s}(r,\beta)$ (red circles). (b) The (approximate) dimension spectrum of the stability index. The maximal dimension 1 is attained at $\sigma = 0.082$, the theoretical value of the index for Lebesgue-typical points. All calculations are performed for the system given by (8) and (9) with parameters $a = 0.45$, $\epsilon = 0.001$, $r = 2$ and order of approximation $N = 21$. The factor s^* from (30) is numerically determined as $s^* = 0.077$.

V. SUMMARY

The manner in which correlations between disparate interacting systems develop is of interest, and the phenomenon of generalized synchronization, which is ubiquitous in nature offers a comprehensive framework for understanding the emergence of such correlations. The formation of dynamical attractors that are in some sense stable arises from the existence of a functional relationship between the variables of the two subsystems.

Here we have exploited the parallels between the transition to WGS when a nonlinear system is driven by a chaotic force,

and the creation of SNA when the drive is quasiperiodic. The theory for chaotically forced systems is poorly developed in comparison to the theory associated with quasiperiodically forced systems. In the present paper we have considered a simple example of the former situation, namely that of a monotone map driven by a chaotic iterative dynamical system. We show that it is possible to calculate the Hausdorff dimension of the set of zeros of the invariant graph and are also able to estimate the stability index that prevails over the set close to the base. The theoretical and numerical estimates of the stability index show quite satisfactory agreement. Transitions in the dimension spectrum in a related system, namely the filtered Baker map driving a one-dimensional dynamical system have been studied earlier [33], also using the thermodynamic formalism. In related [22,26] and future work we aim to study these connections in greater detail, and extend this analysis to higher dimensions as well as to continuous dynamical systems.

ACKNOWLEDGMENTS

H.H.J. would like to thank the CSIR, India for support through a senior research fellowship. R.R. acknowledges support from the Department of Science and Technology, India, through a J. C. Bose fellowship. G.K. is supported by a grant of the German Research Council (DFG).

[1] C. Huygens, *The Pendulum Clock* (Iowa State University Press, Ames, 1986).
[2] H. Fujisaka and T. Yamada, Prog. Theor. Phys. **69**, 32 (1983); T. Yamada and H. Fujisaka, *ibid*. **70**, 1240 (1983).
[3] L. M. Pecora and T. L. Carroll, Phys. Rev. Lett. **64**, 821 (1990).
[4] M. G. Rosenblum, A. S. Pikovsky, and J. Kurths, Phys. Rev. Lett. **76**, 1804 (1996).
[5] Y. Kuramoto, *Chemical Oscillations, Waves, and Turbulence* (Springer-Verlag, Berlin, 1984).
[6] L. M. Pecora and T. L. Carroll, Phys. Rev. Lett. **80**, 2109 (1998).
[7] K. Josic, Phys. Rev. Lett. **80**, 3053 (1998).
[8] N. F. Rulkov, M. M. Sushchik, L. S. Tsimring, and H. D. I. Abarbanel, Phys. Rev. E **51**, 980 (1995).
[9] Z. Zheng, X. Wang, and M. C. Cross, Phys. Rev. E **65**, 056211 (2002).
[10] K. Pyragas, Phys. Rev. E **54**, R4508 (1996).
[11] B. R. Hunt, E. Ott, and J. A. Yorke, Phys. Rev. E **55**, 4029 (1997).
[12] C. Grebogi, E. Ott, S. Pelikan, and J. Yorke, Physica D **13**, 261 (1984).
[13] A. Prasad, S. S. Negi, and R. Ramaswamy, Int. J. Bifurcat. Chaos **11**, 291 (2001); A. Prasad, A. Nandi, and R. Ramaswamy, *ibid.* **17**, 3397 (2007).
[14] T. U. Singh, A. Nandi, and R. Ramaswamy, Phys. Rev. E **78**, 025205 (2008).
[15] G. Keller, Fund. Math. **151**, 139 (1996).
[16] Z. I. Bezhaeva and V. I. Oseledets, Funct. Anal. Appl. **30**, 223 (1996).
[17] R. Sturman and J. Stark, Nonlinearity **13**, 113 (2000).
[18] J. F. Heagy and S. M. Hammel, Physica D **70**, 140 (1994).
[19] T. Nishikawa and K. Kaneko, Phys. Rev. E **54**, 6114 (1996).
[20] A. Prasad, V. Mehra, and R. Ramaswamy, Phys. Rev. Lett. **79**, 4127 (1997).
[21] T. Yalçinkaya and Y. C. Lai, Phys. Rev. Lett. **77**, 5039 (1996).
[22] G. Keller and A. Otani, arXiv:1208.2888 [math.DS] (to be published in Dynamical Systems).
[23] L. Barreira and B. Saussol, Trans. Amer. Math. Soc. **353**, 3919 (2001).
[24] L. Olsen, J. Math. Pures Appl. **82**, 1591 (2003).
[25] O. Podvigina and P. Ashwin, Nonlinearity **24**, 887 (2011).
[26] G. Keller, arXiv:1209.2287 [math.DS].
[27] D. Ruelle, Trans. Amer. Math. Soc. **185**, 237 (1973); P. Walters, Amer. J. Math. **97**, 937 (1975).
[28] P. Billingsley, Illinois J. Math. **4**, 187 (1960).
[29] D. Simpelaere, Acta Appl. Math. **57**, 133 (1999).
[30] R. Bowen, Trans. Amer. Math. Soc. **154**, 377 (1971).
[31] I. S. Gradshteyn and I. M. Ryzhik, *Table of Integrals, Series, and Products* (Academic Press, New York, 1980), see formula (4.224.9).
[32] G. Keller, Stoch. Proc. Appl. **71**, 187 (1997).
[33] P. Paoli, A. Politi, and R. Badii, Physica D **36**, 263 (1989).